

BNL-67322

FORMATION MECHANISMS AND CHEMICAL CHARACTERISTICS OF ELEVATED  
PHOTOCHEMICAL LAYERS OVER THE NORTHEAST UNITED STATES

April 2000

Published in  
Journal of Geophysical Research  
[vol. 103, 10,631-10,647, 2000]

By acceptance of this article, the publisher and/or recipient acknowledges the U.S. Government's right to retain a nonexclusive, royalty-free license in and to any copyright covering this paper.

Research by BNL investigators was performed under the auspices of the U.S. Department of Energy under Contract No. DE-AC02-98CH10886.

## Formation mechanisms and chemical characteristics of elevated photochemical layers over the northeast United States

Carl M. Berkowitz,<sup>1</sup> Jerome D. Fast,<sup>1</sup> Stephen R. Springston,<sup>2</sup> Richard J. Larsen,<sup>3</sup> Chester W. Spicer,<sup>4</sup> Paul V. Doskey,<sup>5</sup> John M. Hubbe,<sup>1</sup> and Robert Plastringer<sup>4</sup>

**Abstract.** The chemical composition of layers of trace gas mixtures within the lower troposphere and their relationship to surface trace gas concentrations are investigated using airborne chemistry and meteorological measurements made over eastern Connecticut and central Massachusetts. Layers of photochemically aged material were identified by maxima above the surface stable layer in the profiles of O<sub>3</sub>, NO<sub>x</sub>, CO, aerosols, peroxyacetyl nitrate (PAN), and the ratio of highly to lesser reactive hydrocarbons (e.g., benzene and toluene). Observations suggest that strong diurnal variations in surface-ozone mixing ratios are associated with elevated layers of ozone and other trace gases. The elevated layers were also associated with strong gradients of NO<sub>x</sub> both vertically, across the mixed layer, and horizontally, between urban and rural regions, providing evidence for the dominant role of localized anthropogenic NO<sub>x</sub> emissions over North America on ozone production in urban regions. On days when elevated layers were detected, isoprene's late-morning propene-equivalent mixing ratio (a measure of nonmethane hydrocarbon reactivity with OH) was an order of magnitude greater than that of the next most reactive species up to an altitude of 650 m mean sea level. Four-dimensional data assimilation was used within a mesoscale model to study the formation mechanism and history of these layers, with a key result being that no unique "age" or source region could generally be attributed to these layers as a consequence of turbulent mixing and transport leading to their formation.

### 1. Introduction

In an effort to better understand the processes associated with high ozone levels, atmospheric chemists often make use of routine observations from a network of surface air-quality monitors that are operated and maintained by a variety of agencies. These surface air chemistry observations, combined with twice-daily National Weather Service (NWS) profiles of wind, temperature, and moisture collected at stations separated by several hundred kilometers still serve as the basic tools for local and regional-scale air-quality studies [e.g., Hanna *et al.*, 1996; Sistla *et al.*, 1996].

Although air-quality monitoring networks provide observations of the spatial and temporal variation of ozone and ozone precursors at the surface, they provide no information about chemistry above the ground. Aircraft observations from the North Atlantic Regional Experiment (NARE) [Fehsenfeld *et al.*, 1996; Kleinman *et al.*, 1996; Berkowitz *et al.*, 1995] and the Southern Oxidants Study (SOS) [Berkowitz and Shaw, 1997] have shown that surface and upper air chemistry are frequently decoupled. As a conse-

quence, surface measurements are generally representative only of what is being measured near the ground. The need for chemical information aloft becomes apparent when one considers that the daytime boundary layer has a typical depth of order 1 km and that chemicals from a much deeper column aloft are likely to be entrained into the growing convective boundary layer.

Not only is there a lack of routine chemical observations aloft, there are insufficient meteorological observations in the northeastern United States to adequately describe boundary layer processes that can bring chemicals aloft down to the surface. The National Weather Service meteorological network was designed to resolve upper air synoptic scale features such as pressure troughs and ridges; however, it cannot adequately resolve mesoscale circulations and boundary layer processes that affect the formation, transport, and fate of ozone and its precursor species.

It is within this context that Pacific Northwest National Laboratory (PNNL), Battelle Memorial Institute (BMI), Brookhaven National Laboratory (BNL), Argonne National Laboratory (ANL), and the Environmental Measurements Laboratory (EML) made a series of airborne chemical and meteorological measurements during the 1995 ozone season along the east coast of North America. The primary scientific objective of this study was to evaluate the effects of turbulent mixing on atmospheric chemistry under conditions of clear skies and light winds during the morning transition from nocturnal stable stratification to the afternoon convective mixed layer. A secondary objective was to make measurements in support of the North American Research Strategy for Tropospheric Ozone (NARSTO) 1995 Northeast field cam-

<sup>1</sup>Pacific Northwest National Laboratory, Richland, Washington.

<sup>2</sup>Brookhaven National Laboratory, Upton, New York.

<sup>3</sup>Environmental Measurements Laboratory, New York.

<sup>4</sup>Battelle Memorial Institute, Columbus, Ohio.

<sup>5</sup>Argonne National Laboratory, Argonne, Illinois.

Copyright 1998 by the American Geophysical Union.

Paper number 97JD03751.  
0148-0227/98/97JD-03751\$90.00

paign [Roberts *et al.*, 1995]. In particular, our data collection effort was designed to help assess the three-dimensional pollutant distribution on episode days and to develop a data base for use in model input and evaluation.

In this paper we describe observations taken on 2 days during which air-quality monitoring stations below an airborne sampling path measured surface ozone levels in excess of 90 ppb, in contrast to the preceding days when mixing ratios did not exceed 50 ppb. Our observations show that high surface ozone mixing ratios having a strong diurnal variation are associated with layers of pollutants aloft, in contrast to days with relatively small, temporally uniform surface ozone mixing ratios that showed little height variation in ozone,  $\text{NO}_x$ , and other species. Profiles of ozone,  $\text{NO}_x$ , nonmethane hydrocarbons (NMHCs), radon, and peroxyacetyl nitrate (PAN) are presented for these conditions.

Meteorological processes were identified using standard National Weather Service soundings, surface observations, wind profilers throughout the region, and analyses produced by a mesoscale modeling system with four-dimensional data assimilation to synthesize these meteorological data sets. Photochemical air monitoring stations were deployed throughout the northeastern United States as a part of the NARSTO '95 field campaign and provided the basis for comparing the aircraft measurements with surface air chemistry measurements.

## 2. Aircraft Measurements

### 2.1. Aircraft Platform and Sampling Procedures

A Grumman Gulfstream-I (G-1) aircraft served as the measurement platform for this study. The aircraft was operated in a nonpressurized configuration because the study was conducted entirely in the lower troposphere and instruments are more readily calibrated when ambient and cabin pressure are the same.

Between August 30 and September 5, 1995, instrumentation onboard the G-1 measured air chemistry and meteorological quantities during a series of horizontal flight segments at various altitudes below 2 km over eastern Connecticut and central Massachusetts (Figure 1). This sampling domain was selected because of its proximity to urban areas associated with high ozone mixing ratios, the absence of strong localized emission sources directly under the flight paths, and the absence of towers or other high-elevation obstructions that would complicate sampling during low-level flight segments. We have removed data collected when the aircraft was making large changes in direction, speed, or altitude since these accelerations are known to complicate the interpretation of instrument performance. A representative flight segment for the remaining data is also shown in Figure 1. With sampling speeds of approximately  $100 \text{ m s}^{-1}$ , each mission had the order of seven to eight horizontal 100-km flight segments of approximately 17-min duration during a 3-hour period. The remaining time was spent in transit or realigning the aircraft for subsequent sampling.

All of the sampling missions, except the first, began within a few hours after sunrise. The first mission (August 30) was carried out during the late afternoon when the mixed layer had already reached its maximum depth. Sampling segments on subsequent days were flown at altitudes that were within and above the developing mixed layer, where the selected

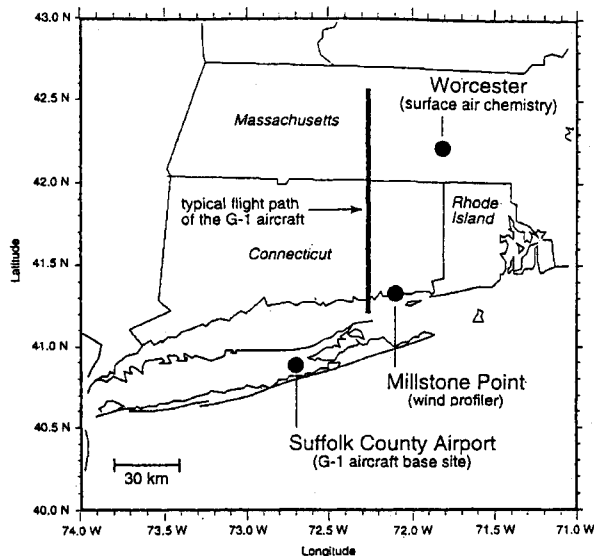


Figure 1. Typical flight path of the G-1 aircraft during the 1995 NARSTO-northeast field campaign and the locations of surface air chemistry and wind profiler measurement sites used in this study.

altitude was determined from profiles of potential temperature, moisture, and subjective estimates of turbulence obtained during preceding flight segments.

Two sets of ancillary observations were available for comparison with the aircraft measurements. A wind profiler/RASS system at Millstone Point, Connecticut (Figure 1), operated by Radian and Sonoma Technology, Inc., provided average wind speed and direction at 44 levels between 115 and 3919 m above ground level (AGL) and instantaneous virtual temperature at 14 levels between 132 and 1497 m AGL at hourly intervals. During the G-1 flight periods, wind and temperature data were usually available within 3 km and 1 km of the ground, respectively. While several routine air quality (the Environmental Protection Agency's Aerometric Information Retrieval System) and photochemical air monitoring stations (PAMS) were located in the area, only the surface air chemistry measurements taken at Worcester, Massachusetts [Korc *et al.*, 1996; Roberts *et al.*, 1995] will be presented and compared with airborne measurements.

### 2.2. Instrumentation

Because several of the noncommercial instruments flown on the G-1 are unique, additional details of their design and operation are presented. Oxides of nitrogen were measured with an instrument designed and constructed at Brookhaven National Laboratory. A forward facing Teflon inlet supplied samples to each of three independent channels which simultaneously measure  $\text{NO}$  by ozone chemiluminescence. Selective conversion of active nitrogen species to  $\text{NO}$  in two of the channels allows additional specificity. The three channels measure  $\text{NO}$ ,  $\text{NO}_2$  by photolytic conversion to  $\text{NO}$ , and the sum of the reactive nitrogen species,  $\text{NO}_x$ , using a hot catalyst for conversion to  $\text{NO}$ . The  $\text{NO}_x$  converter is a Pyrex tube (2.5-cm diameter x 10 cm) loosely packed with approximately

15 g of molybdenum screen ( $40 \times 40$  wires  $\text{cm}^{-1}$ ) and heated to  $350^\circ\text{C}$  at ambient pressure. Automatic zeros were taken in flight at 10-min intervals using a prereactor to remove all NO before the reaction chamber. Standard additions of NO and  $\text{NO}_2$  in ambient air were also performed to assess the instrument response (3 channels) and converter efficiency (for two channels) under flight conditions. Both the instrument response and the converter efficiencies agreed well with ground determinations and were not significantly affected by altitude, ambient humidity, or ozone concentration.

The basic converter design used in the  $\text{NO}_x$  channel has been tested for conversion efficiency with  $\text{NO}_2$ ,  $\text{HNO}_3$ ,  $\text{NH}_3$ , HCN, RCN, and organic nitrates [Nunnermacker, 1990]. The converter actually used in this program has been changed slightly in that the Pyrex tube is now centered inside an outer ceramic sleeve that is then wound with heating wire rather than directly wrapping the tube itself. A thermocouple sensor is cemented to the surface of the Pyrex tube. This configuration provides for more even heating of the converter and eliminates "hot spots" which caused the molybdenum to slowly decompose.

Carbon monoxide was measured with a commercial instrument (Model 48, Thermo Environmental Instruments, Franklin, Massachusetts) that was modified for enhanced sensitivity and stability. The detection threshold has been improved to approximately 10 to 20 ppbv for a 30-s sampling period (based in part on Dickerson and Delany [1988]). Additional modifications include pressurization of the flow cell to a constant  $2 \times 10^5$  Pa, active flow control at a constant  $1.25 \text{ L min}^{-1}$ , and independent temperature stabilization of the flow cell and photo detector. Automatic zeros were taken in flight at 10-min intervals based on removal of CO with a catalyst.

Peroxyacetyl nitrate (PAN) was measured by gas chromatography using a Shimadzu GC-Mini 2 gas chromatograph equipped with a 30-m Restek RTX 200 fused silica capillary column and a  $^{63}\text{Ni}$  electron capture detector. The instrument was equipped with an electrically actuated gas sampling valve and a special thermoelectric cold trap and controller for pre-concentration of PAN in the air sample. The GC column was operated at  $45^\circ\text{C}$  and the detector was set at  $55^\circ\text{C}$ . The carrier gas was methane (10%) in argon. A Hewlett-Packard Model 3390A reporting integrator was used to process the signal from the detector. Sampling was accomplished through the use of a pump to continuously draw air from the aircraft manifold through a Teflon filter and 1/8-inch Teflon tubing to the inlet of the gas sampling valve. From this point, a mass flow controller and pump were used to draw an exact volume of air through the cold trap. The controller automatically collected and analyzed a sample every 8 min. The detection limit for PAN was approximately 15 ppt. Multi-point calibrations using PAN samples were performed at the beginning and end of the field project using the calibration procedures described by Holdren and Spicer [1984]. Daily quality control checks made use of a 607-ppt standard of n-propyl nitrate. The precision of the analysis, based on the repetitive quality control checks, was  $\pm 2\%$ .

Nitric acid and nitrous acid measurements were made with a Sciex Model 6000E tandem mass spectrometer that was specially modified for aircraft sampling [Spicer et al., 1994a]. The mass spectrometer sampled air provided by ram flow through a stainless steel probe mounted outside the aircraft

cabin. Approximately 2 m of 1.9-cm diameter Teflon tubing connected the mass spectrometer to the probe. The flow rate of  $1000 \text{ cm}^3 \text{ s}^{-1}$  provided a residence time of about 0.5 s in the sample tube. Chloride was used as the reagent ion. Chloride forms an adduct with acids [Spicer et al., 1994b; Davidson et al., 1980]. Detection limits are approximately 0.5 ppb for HONO and 0.1 ppb for  $\text{HNO}_3$ . The linearity of the mass spectrometer was determined through multipoint calibrations. Single-point calibrations were performed before and after each flight by adding known levels of the acids to a flowing ambient air sample while monitoring the change in response. The acids were generated using permeation tubes. The accuracy of calibration is estimated at 20%, and the measurement precision is estimated at 10%.

Samples for nonmethane hydrocarbon (NMHC) analysis were collected in Summa<sup>®</sup> passivated stainless steel canisters (Scientific Instrumentation Specialists, Moscow, Idaho). The canisters were cleaned in a series of pressurization/evacuation cycles using humidified zero-grade air, evacuated to  $<0.2$  mm Hg, and shipped to the field. The pressure in each canister was checked in the field immediately before sample collection. Ambient air that flowed through a forward-facing stainless steel inlet was pressurized in the canisters using a metal bellows pump.

The NMHC samples were analyzed by procedures that have been presented in detail by Doskey [1991] and Fukui and Doskey [1996]. The analytic system consisted of a sample concentrator (Chemical Data Systems CDS 330; Autoclave Inc., Oxford, Pennsylvania) and a Hewlett-Packard HP 5890A high-resolution gas chromatograph (HRGC) with a flame ionization detector (FID). Samples were injected at  $40 \text{ mL min}^{-1}$  into the preconcentrator through a glass-lined stainless steel inlet. The NMHCs were cryogenically pre-concentrated in a glass-lined stainless steel tube ( $16 \text{ cm} \times 0.318 \text{ cm}$ , outer diameter) packed with 60/80-mesh porous glass beads (Unibeads 1S; Alltech Associates, Inc., Deerfield, Illinois) at  $-100^\circ\text{C}$  and then were thermally desorbed from the trap for 2 min at  $100^\circ\text{C}$ . The sample concentrator was interfaced to the HRGC with an uncoated, deactivated fused-silica transfer line ( $0.53 \text{ mm} \times 1.2 \text{ m}$ ). A glass union (J&W Scientific, Folsom, California) was used to connect the transfer line to the analytic column. The transfer line was maintained at  $60^\circ\text{C}$ .

The NMHCs were separated on a 60 m long by 0.32 mm inner diameter fused-silica capillary column coated with a  $1\text{-}\mu\text{m}$  film of DB-1 (J&W Scientific, Folsom, California). The entire analytic system was cleaned each day by using an on-line source of humidified helium as the purge gas. An instrument blank was determined by using the same humidified helium. The NMHCs were quantified with National Institute of Standards and Technology (NIST) standard SRM 1665b, containing propane at  $2.87 \pm 0.03$  ppmv in air and a certified gas standard mixture of  $\text{C}_2\text{-C}_6$  hydrocarbons at a level of 10 ppbv in zero air (Scott Specialty Gases, Plumsteadville, Pennsylvania). Recoveries for  $\text{C}_2\text{-C}_6$  NMHC standards in static dilution bottles and canisters by this method are greater than 90% [Doskey, 1991]. The detection limit for NMHCs in a 500 mL is 0.01 ppbC, and the precision for the NMHCs is about  $\pm 5\%$ .

Radon-222 is a radioactive gas with a half-life,  $\tau_{1/2}$ , of 3.8 days. Because it is uniquely produced from the decay of  $^{226}\text{Ra}$  within the Earth's crust, it is a good tracer of air origi-

nating within the boundary layer. Results come from a newly designed instrument that makes measurements of charged  $^{218}\text{Po}$  from which  $^{222}\text{Rn}$  concentrations are derived [Negro *et al.*, 1996]. Polonium-218 is produced by the decay of  $^{222}\text{Rn}$  and, because of its short half-life ( $\tau_{1/2} \approx 3$  min), represents ambient  $^{222}\text{Rn}$  concentrations. Details of the measurement techniques are given by Lee and Larsen [1997].

### 3. Meteorological and Particle Dispersion Simulations

The Regional Atmospheric Modeling System (RAMS, version 3a) [Pielke *et al.*, 1992] and a Lagrangian Particle Dispersion Model (LPDM) are used to describe the atmospheric flow features that affect pollutant transport and diffusion during the G-1 flight periods. Details of the parameterizations employed by both models are given by Fast and Berkowitz [1996]. We use RAMS to provide physically consistent analyses of the meteorological fields in time and space, and use the LPDM to quantitatively describe specific features of these fields.

In this study, a nested grid configuration was used in RAMS in which the outer grid encompasses most of the United States and southern Canada east of the Rocky Mountains with a horizontal grid spacing of 48 km. Two 4.5-day simulations were performed. One was initialized at 0700 LT, August 28 and the other at 0700 LT, September 2. The initial conditions and lateral boundary conditions are based on large-scale analyses from the National Center for Environmental Prediction (NCEP) Aviation model and rawinsonde observations. A second grid that encompasses southern Quebec, eastern New York, eastern Pennsylvania, New Jersey, and most of New England with a horizontal grid spacing of 12 km is added 2 days into the simulation period. To resolve flows influenced by land-sea contrasts and local topography in the vicinity of the G-1 flight paths, a third grid that encompasses Long Island, Connecticut, Rhode Island, and western Massachusetts with a horizontal grid spacing of 3 km is added 3 days into the simulation period. All three grids employ a stretched terrain-following vertical coordinate with a grid spacing of 50 m adjacent to the surface. The grid spacing is 100 m between 50 and 1550 m above ground (AGL) above which the spacing gradually increases to 1000 m near the model top at an elevation of 17.9 km AGL. Owing to the staggered coordinate system, the lowest model vertical coordinate is located about 26 m AGL. This nested grid configuration can represent synoptic-scale, mesoscale, and boundary layer processes associated with pollutant transport over the northeastern United States.

We have noted in the introduction the limitations of synoptic-scale meteorological observations for identifying local circulations. Anticipating that these smaller-scale features would be important, we employed a four-dimensional data assimilation technique in RAMS [Fast, 1995] to bring the  $u$  and  $v$  components of the wind, potential temperature, and specific humidity into closer agreement with the additional meteorological observations collected during the field campaign. Rawinsonde observations (at 0700 and 1900 LT) and hourly data from wind profilers, sodars, and surface stations measured during the 1995 NARSTO-Northeast field campaign [Korc *et al.*, 1996] are incorporated into the model results throughout the 4.5-day simulation period, thereby

reducing the uncertainties associated with pollutant transport. The mesoscale model results are therefore a blend of the predicted and observed variables when and where the observations occur. In data sparse regions, only the model governing equations are used to predict the flow field. For example, the model results on the innermost nested grid are influenced by rawinsondes near Albany and eastern Long Island, New York, a wind profiler and sodar near Millstone Point, Connecticut (Figure 1), and about 30 surface meteorological observations.

The mean wind fields and the turbulent quantities determined by the mesoscale model at 1-hour intervals are used to drive the LPDM. The LPDM linearly interpolates the mean and turbulent quantities in time during individual 1-hour periods using a time step of 15 s. Particles are non-buoyant and a perfect reflection of particles occurs at the ground; deposition is not included in this study. Each particle is tagged by its release location and release time so that the history of a particle plume can be obtained to determine the atmospheric mechanisms associated with pollutant transport and diffusion during the G-1 aircraft flight periods. The 4.5-day simulation period enables the individual particles to be tracked for a substantial period of time, so that long-range transport and the "age" of the particle plume over Connecticut can be derived. Twenty-nine release locations are employed, corresponding to the largest metropolitan areas east of the Mississippi River. Particles are emitted during daylight hours at a constant rate within an area of 2304 km<sup>2</sup> centered over each metropolitan area and within 26 m of the ground. Particle release rates are not scaled to local emission rates since ozone, the focus of our study, forms from a complicated mix of predecessor nitrogen and hydrocarbon compounds. The emission rates for these compounds are highly uncertain and would require selecting one such species as the single representative predecessor. A constant release rate is appropriate in developing estimates of transport times, identification of source regions, or descriptions of the formation mechanisms of the layers to be considered. Approximately 335,000 particles are released over the 4.5-day period. This emission scenario does not consider pollutants released from every urban area and industrial point source within the domain; nevertheless, there are a sufficient number of release locations to determine possible source regions for the pollutants observed by the G-1 over Connecticut.

### 4. Analysis Techniques and Results

Our analysis is focused on August 31 and September 5, corresponding to flight days when the surface mixing ratio of ozone was significantly higher than on preceding days (August 30 and September 4). Mean values measured on all segments, for all missions, are listed in Tables 1 and 2.

Profiles have been constructed with the assumption that mean values measured along flight segments made within ~90 min of each other can be combined to characterize the vertical structure of the region bounded by the southern and northern ends of the segment. Two considerations justified this approach. We found the structure of these time-averaged profiles to be similar to profiles constructed from aircraft spirals where the time between maximum and minimum altitude was less than 5 min, suggesting that the general features were relatively stationary during sampling. Further justification comes from noting that the time-averaged profiles constructed from early morning flight segments were similar

**Table 1.** Mean Values Measured Along the Flight Segments Shown in Figure 1 During the 1995 NARSTO Campaign

Seg. I.D.	Start, LT	Stop, LT	Meters, MSL	$\sigma^2_{\theta}$ , °C <sup>2</sup>	T <sub>dp</sub> , °C	O <sub>3</sub> , ppb	CO, ppb	ASASP Counts, cm <sup>-3</sup> s <sup>-1</sup>	222RN, Bq m <sup>-3</sup>
<b>Aug. 30</b>									
2	1408:09	1426:28	1905	0.005	-22.8	41	136	105	NA
4	1429:53	1447:06	655	0.003	4.8	47	134	352	NA
6	1447:47	1504:23	394	0.007	5.4	40	138	346	NA
8	1512:15	1526:52	2554	0.001	-22.5	40	147	130	NA
<b>Aug. 31</b>									
2	0759:09	0819:50	1285	0.001	1.3	50	184	918	NA
4	0823:47	0840:02	664	0.002	4.0	37	147	442	NA
6	0841:37	0857:04	393	0.016	9.4	32	190	590	NA
8	0859:11	0917:15	970	0.002	10.1	61	269	2187	NA
10	0923:18	0935:36	503	0.012	9.4	27	212	718	NA
12	0939:02	0954:29	1289	0.001	4.4	37	199	2068	NA
14	0956:51	1013:21	652	0.009	10.1	33	245	1460	NA
16	1016:47	1031:42	972	0.012	11.7	45	265	3783	NA
<b>Sept. 1</b>									
3	0800:31	0827:55	1289	0.009	-7.8	41	NA	196	0.99
5	0831:42	0854:38	658	0.022	13.4	38	NA	766	2.26
7	0857:33	0921:34	365	0.006	15.1	36	149	827	2.43
11	0931:04	0953:43	1280	0.006	-6.5	40	114	226	1.43
13	0956:24	1025:58	638	0.012	13.6	39	141	728	2.08
15	1028:44	1037:46	1435	0.003	7.8	39	131	473	2.19
17	1041:47	1054:24	1413	0.004	-11.1	37	101	88	0.99
<b>Sept. 3</b>									
3	0820:34	0848:07	1271	0.001	1.1	34	139	549	0.80
5	0851:43	0917:05	395	0.007	7.3	91	147	659	1.77
7	0921:01	0947:24	1280	0.002	1.1	34	150	559	0.94
9	0950:10	1014:04	423	0.008	6.2	35	144	592	1.66
11	1022:46	1043:37	1888	0.01	-5.6	34	150	272	0.64
13	1047:18	1111:26	962	0.003	4.3	36	146	599	1.36
<b>Sept. 4</b>									
3	0800:46	0819:18	902	0.001	5.7	43	233	1353	1.03
5	0822:38	0838:48	421	0.024	9.1	48	232	1645	1.13
7	0840:57	0959:48	926	0.001	6.9	47	226	1452	0.94
9	0903:07	0920:21	427	0.018	11.8	45	263	1779	1.86
11	0923:24	0941:36	1235	0.001	5.1	42	199	1062	1.18
13	0944:54	1002:29	611	0.006	9.9	49	236	1599	1.52
15	1007:11	1024:25	1852	0.001	2.2	36	166	514	1.12
17	1027:13	1046:58	908	0.003	8.8	48	225	1578	1.48
<b>Sept. 5</b>									
2	0803:32	0829:17	1877	0.001	7.3	58	217	3293	1.19
4	0834:10	0845:45	439	0.004	15.5	39	264	1986	1.44
6	0849:08	0905:29	944	0.003	10.9	62	284	3674	1.27
8	0909:28	0924:39	398	0.006	16.2	39	260	2293	1.61
10	0927:45	0944:42	1261	0.001	9.2	59	235	3171	1.64
12	0947:46	1004:58	619	0.005	15.4	45	285	2768	1.45
14	1009:03	1026:16	1874	0.001	6.6	48	215	1961	1.74
16	1029:48	1056:38	387	0.008	16.6	45	279	2653	1.64

"Seg I.D." is the flight segment identification number used in the text, "start" and "stop" LT are the associated (local time) starting and stopping times. "Alt." is the altitude in meters above mean sea level. The parameter  $\sigma^2_{\theta}$ , is the variance of the high-frequency potential temperature signal (see text). The parameter "T<sub>dp</sub>" is the dew point in Centigrade. ASASP refers to dry accumulation mode aerosols (diameters between 0.1 and 3  $\mu\text{m}$ ).

to those made later in the day, although the later tended to be more uniform and have maximum values less than those found in the earlier profiles. This too suggests small changes in the key features to be identified during the ~90 min sampling periods.

In the analysis to follow, we distinguish between data collected within and above the mixed layer by using the variance,  $\sigma^2$ , of the high-frequency potential temperature,  $\theta' = \theta - \langle\theta\rangle_{3\sigma}$ , as a measure of local convective activity

[Berkowitz and Shaw, 1997]. Large values of  $\sigma^2_{\theta}$  are assumed to be associated with convective eddies and relatively small values indicative of either stable layers or residual layers not associated with mixing during the time of sampling.

We will present the NMHC data in two ways. The first is a simple ranking by mixing ratio,  $r$ . The second presentation sorts the species by their relative reactivity, taking into account not only the relative abundance of the species in

**Table 2.** Mean and Standard Deviations (x/s) of Nitrogen Species Measured Along the Flight Segments Shown in Figure 1

Seg. I.D.	NO, ppb	NO <sub>2</sub> , ppb	PAN, ppb	HNO <sub>3</sub> , ppb	NO <sub>y</sub> , ppb	Σ, ppb
<b>Aug. 30</b>						
2	0.1 / 0.2	0.3 / 0.3	0.3 / 0.1	NA / NA	0.7 / 0.4	0.7
4	0.1 / 0.1	0.6 / 0.3	0.7 / 0.2	NA / NA	1.9 / 0.3	1.4
6	0.1 / 0.1	0.6 / 0.2	1.0 / 0.2	NA / NA	2.2 / 0.3	1.7
8	0.1 / 0.1	0.1 / 0.1	0.3 / 0.0	NA / NA	0.6 / 0.2	0.5
<b>Aug. 31</b>						
2	0.1 / 0.1	0.5 / 0.2	1.7 / 1.0	.98 / .44	3.6 / 1.8	3.3
4	0.4 / 0.9	0.8 / 0.7	1.1 / 0.4	1.14 / .43	3.8 / 3.0	3.4
6	1.8 / 1.7	2.7 / 2.2	0.9 / NA	.95 / .65	7.2 / 4.3	6.3
8	0.1 / 0.1	0.9 / 0.3	3.6 / 0.3	1.64 / .36	8.2 / 1.7	6.2
10	1.5 / 0.8	2.9 / 1.2	2.1 / 1.5	NA / NA	8.8 / 2.5	NA
12	0.1 / 0.0	0.5 / 0.1	2.3 / 0.1	NA / NA	5.3 / 1.0	NA
14	1.3 / 0.6	2.9 / 0.9	2.5 / 0.9	NA / NA	11.1 / 1.5	NA
16	0.2 / 0.2	1.2 / 0.5	3.6 / NA	NA / NA	10.4 / 1.9	NA
<b>Sept. 1</b>						
3	NA / NA	NA / NA	0.2 / 0.1	.10 / .09	NA / NA	NA
5	NA / NA	NA / NA	0.4 / 0.1	-.02 / .03	NA / NA	NA
7	0.6 / 0.3	1.5 / 0.5	0.8 / 0.3	.71 / .05	4.0 / 1.1	3.6
11	0.1 / 0.1	0.1 / 0.1	0.3 / 0.2	.40 / .23	0.9 / 0.1	0.9
13	0.3 / 0.2	1.2 / 0.5	1.0 / 0.2	.64 / .11	3.6 / 1.1	3.1
15	-0.0 / 0.0	0.2 / 0.1	0.7 / NA	.38 / .02	1.2 / 0.1	1.3
17	0.1 / 0.1	0.1 / 0.1	0.2 / NA	.08 / .06	0.9 / 0.3	0.5
<b>Sept. 3</b>						
3	0.0 / 0.0	0.2 / 0.1	0.5 / 0.1	NA / NA	1.1 / 0.1	0.7
5	0.3 / 0.3	0.7 / 0.4	0.6 / 0.0	NA / NA	2.3 / 0.8	1.6
7	0.0 / 0.0	0.1 / 0.1	0.5 / 0.1	NA / NA	1.2 / 0.1	0.6
9	0.2 / 0.2	0.5 / 0.4	0.6 / 0.2	NA / NA	2.0 / 0.7	1.3
11	0.0 / 0.0	0.1 / 0.1	0.4 / 0.1	NA / NA	0.8 / 0.1	0.5
13	0.1 / 0.1	0.3 / 0.1	0.7 / 0.1	NA / NA	1.6 / 0.3	1.1
<b>Sept. 4</b>						
3	0.3 / 0.2	1.0 / 0.6	NA / NA	NA / NA	4.2 / 1.8	NA
5	0.4 / 0.3	1.4 / 0.7	NA / NA	NA / NA	5.2 / 1.1	NA
7	0.2 / 0.1	0.6 / 0.4	NA / NA	NA / NA	4.1 / 1.4	NA
9	0.5 / 0.5	1.5 / 0.7	1.7 / NA	NA / NA	5.5 / 1.6	3.7
11	0.0 / 0.0	0.3 / 0.1	1.2 / 0.2	NA / NA	2.5 / 0.6	1.5
13	0.3 / 0.2	1.0 / 0.8	1.5 / 0.7	NA / NA	4.6 / 1.4	2.8
15	0.0 / 0.0	0.1 / 0.1	0.5 / 0.1	NA / NA	1.3 / 0.1	0.6
17	0.1 / 0.1	0.5 / 0.2	1.7 / 0.5	NA / NA	3.6 / 0.9	2.3
<b>Sept. 5</b>						
2	0.0 / 0.0	0.3 / 0.1	2.3 / 0.7	1.8	3.9 / 0.9	2.6
4	2.0 / 0.7	5.3 / 1.6	0.8 / NA	3.2	10.9 / 2.7	8.1
6	0.1 / 0.1	0.8 / 0.2	3.0 / 0.2	4.7	6.1 / 0.4	3.9
8	2.0 / 0.6	4.5 / 1.2	0.9 / 0.2	2.0	11.2 / 2.3	7.4
10	0.1 / 0.1	0.4 / 0.3	2.2 / 0.6	3.7	4.5 / 0.9	2.7
12	1.6 / 0.7	3.9 / 1.5	1.5 / 0.4	2.2	11.1 / 2.6	7.0
14	0.0 / 0.0	0.2 / 0.1	1.4 / 0.0	1.4	3.0 / 0.1	1.6
16	1.5 / 1.0	4.7 / 2.3	1.4 / 0.5	2.4	11.4 / 4.3	7.6

Also shown is the summation of the mean values of the individually measured components of NO<sub>y</sub>, Σ = NO + NO<sub>2</sub> + PAN + HNO<sub>3</sub>. Parameters shown in this table frequently had a standard deviation comparable to the mean value. HONO was below the detection limit of 0.5 ppb. Related values are given in Table 1.

question, but their potential contribution to the formation of additional ozone, which is approximated by

$$\frac{d[\text{O}_3]}{dt} = [\text{OH}][\text{HC}_i]k_{\text{OH},i} \quad (1)$$

where [OH] and [HC<sub>i</sub>] are the number density of OH and NMHC species *i*, and *k*<sub>OH,*i*</sub> is the rate constant for the reaction between OH and species *i* [Carter and Atkinson, 1987, 1989]. An abundant NMHC with a relatively small reactivity or ozone production efficiency could make a smaller contri-

bution to the production of ozone than a less common, although reactive, NMHC having a greater production efficiency.

Others [e.g., Chameides *et al.*, 1992] have ranked the relative importance of NMHCs having a wide range of reactivities by presenting the concentration required to produce an oxidation rate equivalent to that of standard species, propene being the common normalizing compound for such calculations. We follow use of this definition of "propene-equivalent" mixing ratio because it facilitates comparison of

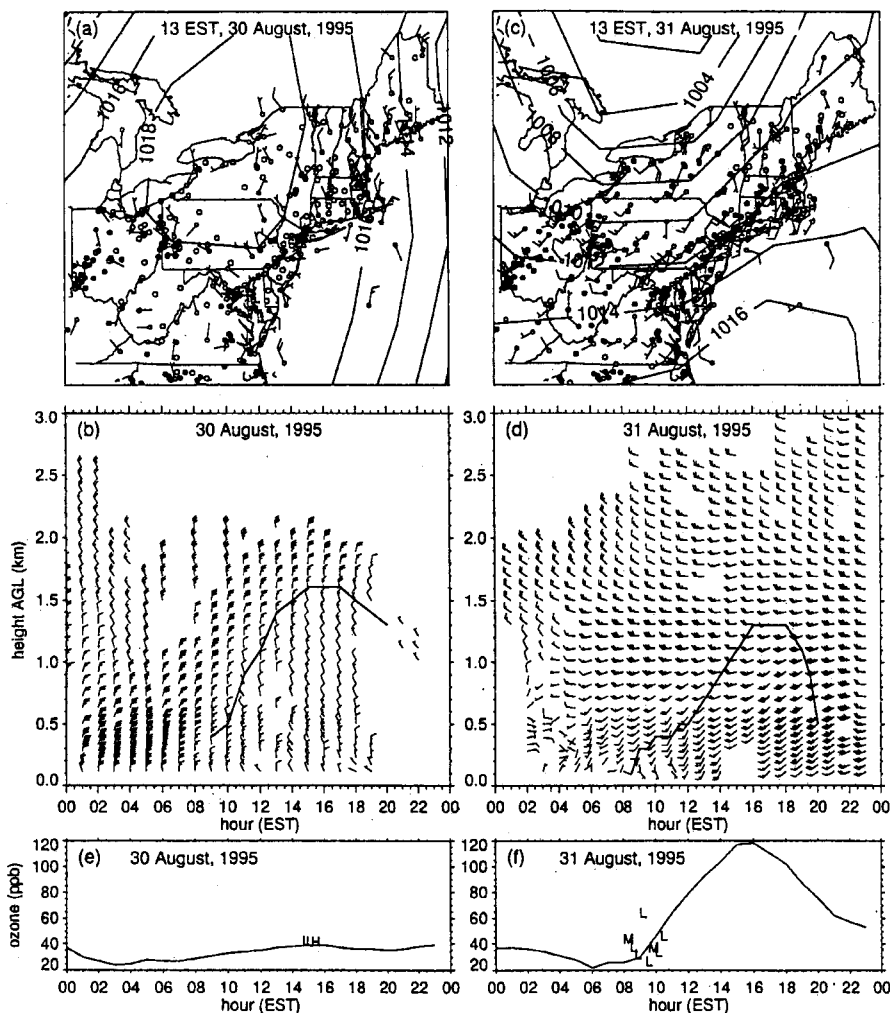


**Figure 2.** Meteorological and surface air chemistry observations on August 30 and 31, 1995. (a) Mean sea level pressure contours (millibars), surface wind vectors, and surface ozone mixing ratios  $>70$  ppb (solid circles) at 1300 LT August 30; (b) profiler wind vectors (full wind barb equal to  $5 \text{ m s}^{-1}$ ) and simulated mixed layer height 75 km north of Millstone Point (thin solid line) on August 30; (c) and (d) same as Figures 2a and 2b, but for August 31; (e) ozone mixing ratio at Worcester (line) and the average ozone mixing ratio along segments of the G-1 flight path on August 30 where "L," "M," or "H" indicate the average mixing ratio measured during low ( $<1$  km MSL), medium (1-2 km MSL), and high ( $>2$  km MSL) altitude flight segments; (f) same as Figure 2e, but for August 31.

our results with those from other investigators, and also because propene was a compound that was always present. The propene-equivalent mixing ratio,  $r_{\text{prop}}$ , is calculated from the mixing ratio  $r_i$ , as

$$r_{\text{prop},i} = r_i \frac{k_{\text{OH},i}}{k_{\text{OH},\text{C}_3\text{H}_6}} \quad (2)$$

Using  $r_{\text{prop},i}$  to estimate the approximate relative contribution each hydrocarbon makes to the local production of ozone presupposes no competition for OH between hydrocarbons, and also that OH is the dominant oxidant. The latter is probably a good assumption for the midmorning sampling reported here, since other oxidants, such as  $\text{NO}_3$ , are absent during daylight hours. Values of  $k_{\text{OH},i}$  were taken from Carter [1990], and DeMore *et al.* [1994].

Although NMHC samples were analyzed for a total of 48 species, we have limited our analysis to the most abundant species sampled over all levels in a given set of flight segments. Thus, if a species was among the top five in abundance at any altitude, it has been included in the analysis. This ranking was done separately for mixing ratio and propene-equivalent mixing ratio.

Mixed layer heights are determined from the simulated turbulent kinetic energy profiles. In the following discussion, these heights are presented for a location 75 km north of Millstone Point. This inland location is likely to be more representative of the convective boundary layer along the G-1 paths than the mixed layer height directly over Millstone Point, which is usually influenced by stable marine air unless there is a significant northerly wind component.

## 4.1. Case 1: August 30-31

The morning of August 30 had high pressure centered over Ottawa, Ontario, that moved to the southeast behind a cold front. Wind speeds behind the cold front diminished by the afternoon, so that weak northerly surface flow was observed over New England by 1300 LT (Figure 2a). Skies were mostly clear over the entire northeastern United States during the afternoon. Profiler observations from Millstone Point (Figure 2b) were consistent with the synoptic pattern showing northerly flow aloft up to 2 km AGL throughout of the day. Also shown in Figure 2b is the simulated mixed layer height. Since there was northerly flow aloft throughout the day, the simulated mixed layer height of approximately 1.6 km AGL between 1500 and 1700 LT was consistent with the profiler observations.

With the passage of the high-pressure system, surface winds that were light and variable over Connecticut in the morning became 3-4 m s<sup>-1</sup> from the southwest by the afternoon of August 31 (Figure 2c). Strong vertical wind shears were observed by the Millstone Point profiler during the morning hours (Figure 2d), with light southerly winds near the surface that became 15 m s<sup>-1</sup> from the west at about 1 km AGL. The near-surface winds became southwesterly during the afternoon and grew in intensity with wind speeds as strong as 18 m s<sup>-1</sup> at about 0.6 km AGL by 1800 LT. The model simulations suggest that the strong southwesterly winds during the afternoon were due to the coupling of the large-scale pressure gradient force (Figure 2c) and the

development of a sea-breeze circulation over Long Island Sound. This mesoscale circulation intensified during the afternoon as the sea-breeze front penetrated inland into Massachusetts by sunset. The model predicted that the convective boundary layer on August 31 (Figure 2d) was weaker than on August 30 (Figure 2b). The mixed layer height grew at a slower rate and reached a maximum height at 1600 LT that was 0.3 km lower than the maximum height on August 30. Late in the afternoon (after 1800 LT), turbulent diffusion was suppressed aloft due to the advection of cooler air within the marine boundary layer by the onshore flow.

Both surface and aircraft observations of ozone showed little variation on August 30 (Figure 2e). Worcester reported nearly constant values of 40 ppb ozone throughout the day, and late afternoon aircraft observations clustered together at 38 ppb. Aircraft sampling on August 30 between 1500 and 1600 LT was within a well-mixed atmosphere under conditions of relatively weak northerly flow. The time series of ozone the next day was quite different (Figure 2f), with ozone concentrations in excess of 100 ppb developing at Worcester (and at many other stations in the region) the afternoon of August 31, in conjunction with surface high pressure moving off the coast of Maryland and Virginia (Figure 2c). Aircraft sampling was done in the morning between 0800 and 1100 LT, in a stratified atmosphere when the mixed layer was shallow and strong vertical wind shears existed.

The differences in the diurnal variation of the surface ozone mixing ratios on August 30 and 31 were associated with changes in synoptic conditions and boundary layer char-

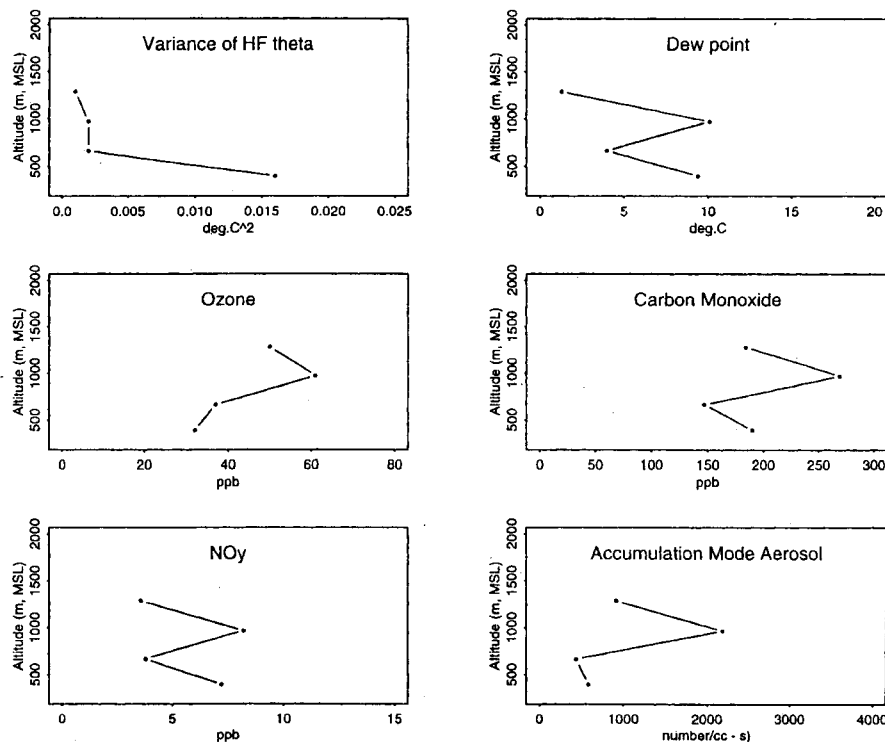


**Figure 3.** Profiles of mean values measured along the flight segments of August 31, 1995. All values are taken within ~90 min of each other. The variance of HF theta refers to the variance of the observed high-frequency potential temperature,  $\sigma^2\theta'$ , used as an indicator of turbulent mixing (see text). Values are plotted for flight segments 6, 4, 8, and 2 (see Tables 1 and 2).

acteristics. Surface ozone observations on August 30 showed little variation during the day (Figure 2e), a feature we attribute to the northerly winds advecting clean air into Connecticut. Whatever ozone and ozone precursors that were present would have been mixed within a deep convective boundary layer, thereby reducing the surface concentrations. In contrast, surface ozone mixing ratios on August 31 began to increase at 0900 LT, with values reaching  $\sim 120$  ppb by 1500 LT. This analysis suggests that the higher ozone mixing ratios on August 31 were a result of southwesterly winds advecting air from regions along the urban east coast corridor into a relatively shallow mixed layer which suppressed vertical mixing of ozone and its precursors.

The aircraft observations are consistent with this description of the vertical structure of the atmosphere. Profiles of the variance of high-frequency potential temperature,  $\sigma^2_{\theta}$ , indicate that sampling during the first part of the morning of August 31 was carried out in a stratified atmosphere showing a vertical gradient in convective activity (Figure 3; top left). The maximum ozone mixing ratio (61 ppb) was detected within a layer of moist air aloft that also had the maximum CO ( $\sim 279$  ppb),  $\text{NO}_x$  (8 ppb), and aerosols ( $2187 \text{ counts cm}^{-3} \text{ s}^{-1}$ ). The benzene/toluene ratio within this layer was 1.2, much greater than values that are typical of recent anthropogenic inputs dominated by vehicle emissions (0.60). Because toluene reacts nearly 5 times faster than benzene with OH (at 298°K), benzene/toluene ratios in vehicle emis-

sions would increase during long-range transport [Doskey and Gaffney, 1992].

While no single measurement alone would indicate the presence of a pollutant layer that had undergone extensive photochemistry, we interpret maxima in the levels of  $\text{O}_3$ , CO,  $\text{NO}_x$ , aerosols, and the benzene/toluene ratio in a thermally stratified atmosphere, as evidence of such a layer. These high concentrations are consistent with what would be found in a photochemically aged air mass coming from urban regions [Daum et al., 1996, and references therein]. Whereas Daum et al. [1996] identified plumes decoupled from the surface following transit over the Gulf of Maine, the layer observed here appears to have been decoupled from the underlying nocturnal boundary layer over land.

Vertical profiles of the most abundant NMHC species and NMHC species with the highest propene-equivalent mixing ratios for the early morning flight segments of August 31 are shown in Plate 1. Ethane is the most abundant species in the NMHC profiles before 0930 LT of August 31 with a mixing ratio nearly twice the value of propane, the next most abundant species. Local maxima in several NMHCs were observed at an altitude consistent with the maxima of other chemical species (Figure 3). The NMHCs other than ethane exhibit a wide range of mixing ratios. The mixing ratio of 2-methylbutane at the lowest altitude was comparable to that of ethane. N-butane, toluene, ethene, acetylene, and propene mixing ratios were also elevated at the lowest altitude, with

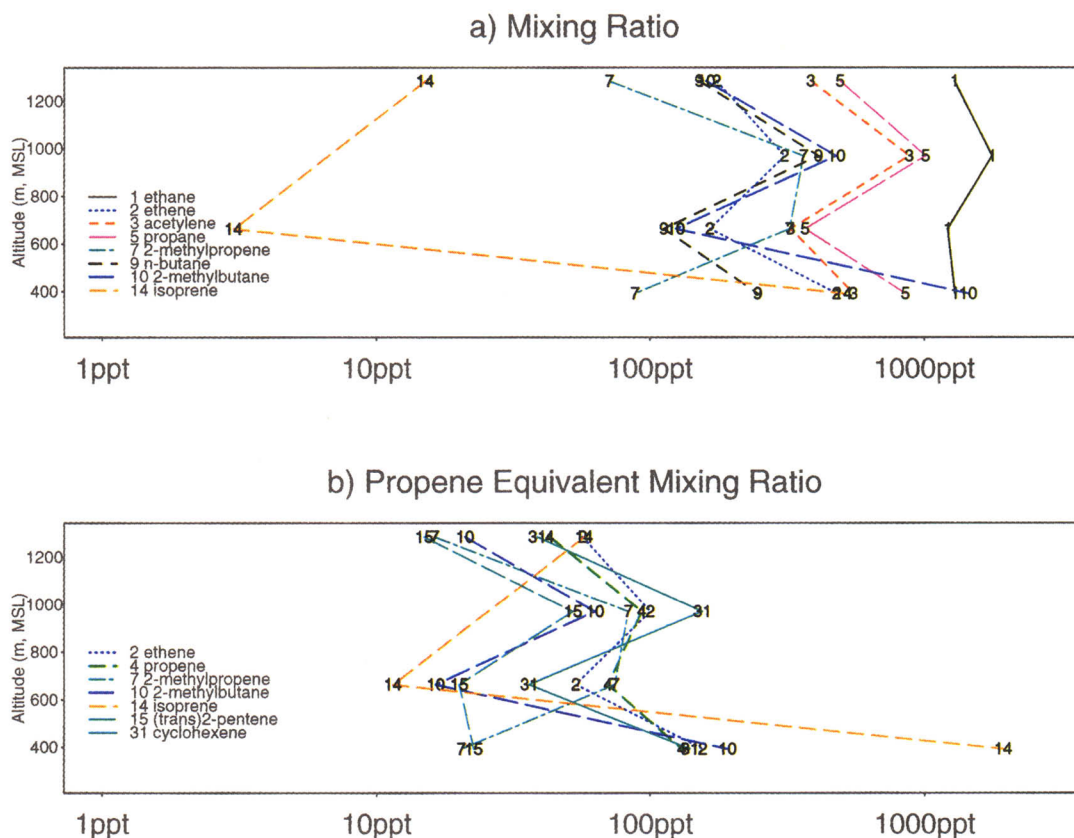


**Plate 1.** Profiles of hydrocarbons that were among the most abundant species at any of the four altitudes sampled before 0930 LT, August 31 1995. (a) "Simple" mixing ratio; (b) "propene-equivalent mixing ratio" (see text). Values are plotted for flight segments 6, 4, 8, and 2 (see Tables 1 and 2). Isoprene measurements were not available at segment 8.

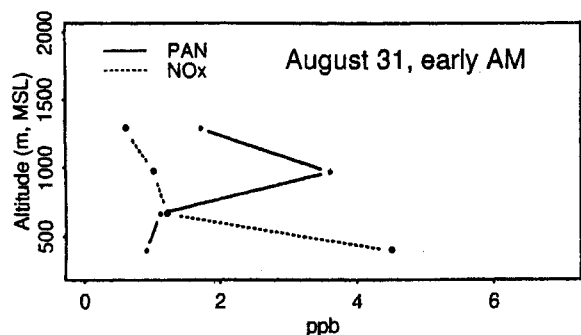


Figure 4. Vertical profile PAN and  $\text{NO}_x$  ( $=\text{NO} + \text{NO}_2$ ), August 31. Values are plotted for flight segments 6, 4, 8, and 2 (see Tables 1 and 2).

the distribution of these NMHCs typical of vehicle emissions. The mixing ratio of isoprene, a biogenic NMHC emission, was also elevated at the lowest altitude. These observations are consistent with the surface emission of anthropogenic and biogenic NMHCs into a shallow nocturnal boundary layer. In contrast to profiles of the NMHC mixing ratios, the propene-equivalent mixing ratios show that the value for isoprene (2000 propene-equivalent ppt) is much greater than the other NMHCs at the lowest altitude. For example, the value for

2-methylbutane, which had the second highest propene-equivalent mixing ratio (190), was an order of magnitude less. These values indicate the relative importance of biogenic emissions to the reactive NMHCs of the boundary layer.

The August 31 NMHC profiles derived from canisters collected after 0930 LT were similar to the early morning profiles in two respects, and different in one key respect. The first similarity was that the mixing ratio of ethane was a factor of 2 greater than propane, the second most abundant species. The second similarity was that although the NMHC maxima at 1000 m were weaker, the same species dominated the mixture at that altitude. The key difference between the late and early morning profiles was the altitude to which isoprene had been mixed into the boundary layer. Isoprene dominated the reactive NMHCs at altitude of 650 m after 0930 LT, attaining a value of 2000 propene-equivalent ppt, an order of magnitude greater than the second most reactive NMHC at and below this altitude (247 propene-equivalent ppt for propene).

Because of the instrument sampling time, each flight segment had no more than three PAN samples. Despite the limited number of samples, we note PAN mixing ratios above the mixed layer on August 31 were greater by a factor of 4 relative to PAN mixing ratios measured at the lowest flight segment (Figure 4). Values were an order of magnitude less throughout the domain during other sampling missions on days with lower surface ozone concentrations. The mixing

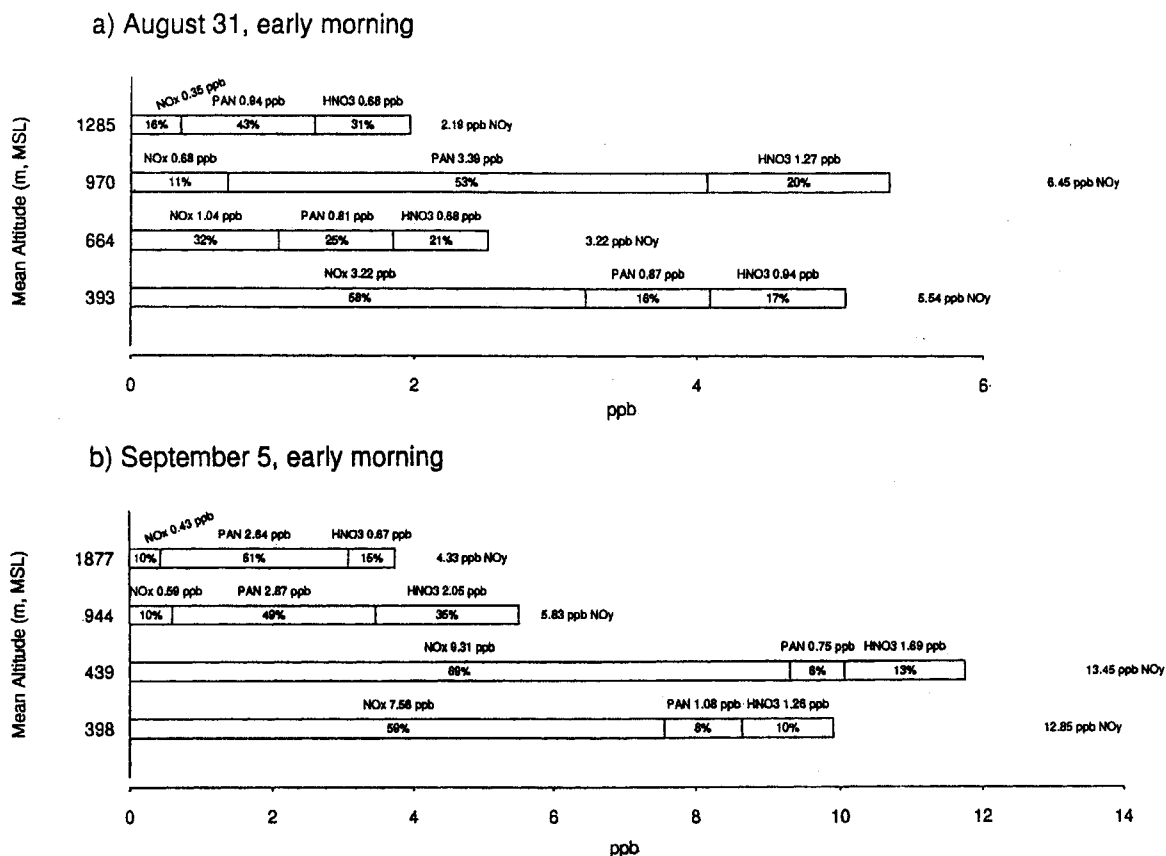
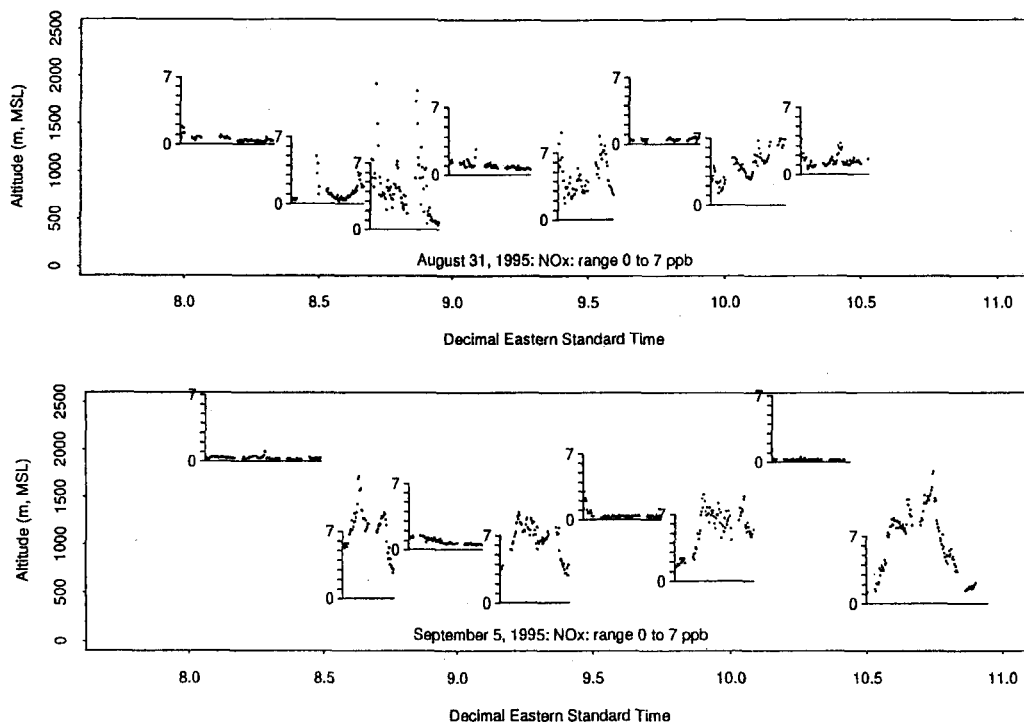


Figure 5. Measured components of total  $\text{NO}_y$  as a function of altitude for (a) August 31, early morning, and (b) September 5, early morning. Values shown were taken within  $\pm 1.5$  min of the PAN samples.



**Figure 6.** Ten second average  $\text{NO}_x$  values for the flight segments of (top) August 31 and (bottom) September 5, with the abscissa of each subplot located at the mean altitude of the segment and the ordinate located over the corresponding time interval.

ratio of the measured components of  $\text{NO}$ , ( $\text{NO}$ ,  $\text{NO}_2$ ,  $\text{HNO}_3$ , and PAN) taken within  $\pm 1.5$  min of the PAN samples, and their fractional contribution to the total  $\text{NO}_x$  for August 31 are shown in Figure 5a. The fractional contribution of  $\text{NO}$  and PAN to the total  $\text{NO}_x$  at the lowest flight segment was  $\sim 60\%$  and  $\sim 15\%$ , whereas the fractional contribution of these species at the highest segment was  $\sim 15\%$  and  $\sim 40\%$ . PAN was the dominant reactive nitrogen species ( $\sim 50\%$ ) within the aged photochemical layer at 970 m.  $\text{NO}_x$  in the presence of sunlight plays an important role in the formation of ozone and is the dominant component of  $\text{NO}_x$  near the surface. PAN is known to thermally decompose into  $\text{NO}_x$  and while not the dominant component of  $\text{NO}_x$  aloft, made up a significant fraction of the total  $\text{NO}_x$ .  $\text{HNO}_3$  has, until recently, been thought to be an end product of ozone photolysis. However, recent work by Rogaski *et al.* [1997] suggests it may form additional  $\text{NO}_x$  through reactions on carbon aerosols. It is beyond the scope of the present study to quantitatively assess the role of PAN and  $\text{HNO}_3$  on the possible enrichment of surface  $\text{NO}_x$  levels, and hence ozone, when aged photochemical layers, such as observed here, are brought to the surface.

In the absence of transport from power plant plumes,  $\text{NO}_x$  would have a source primarily at the surface, with the local variations in  $\text{NO}_x$  emissions and turbulence contributing to the large variability seen along the aircraft flight segments. Mixing ratios varied by factor of 4.5 between segments within and above the mixed layer (Figure 4). The  $\text{NO}_x$  mixing ratios aloft were comparable to boundary layer  $\text{NO}_x$  concentrations measured in rural regions over much of North America, in contrast to typical values in urban or suburban regions that

are 5 to 1000 times greater. Although little variability was seen in the  $\text{NO}_x$  measurements during the higher flight segments, a high degree of variability in  $\text{NO}_x$  was observed along the lower segments (Figure 6). The latter observation is consistent with the day to day, site to site, and urban/suburban variation noted by others with surface observations [Chameides *et al.*, 1992, and references therein].  $\text{NO}_x$  concentrations thus decrease sharply, not only as one moves out of urban regions along the surface, but also upward, providing additional evidence for the dominant role of anthropogenic  $\text{NO}_x$  emissions over North America on the production of ozone in urban areas.

A second set of profiles made after 0930 LT on August 31 showed that while maximum values of  $\text{O}_3$ ,  $\text{CO}$ ,  $\text{NO}_x$ , and aerosols were at an altitude of 1 km, the gradient was not as large as that detected earlier. Suspecting these changes were associated with the onset of turbulent convection, we used the particle dispersion model to investigate how convective processes would affect the elevated layer, and also to determine the source regions of the pollutants within this layer.

Simulated particle concentration profiles were obtained within a sampling volume that extended 48 km to the east and west of the G-1 flight paths. The resulting profiles during the morning hours of August 31 are shown in Figure 7. The modeling system produced a peak concentration between 0.6 and 0.9 km AGL, which was slightly lower than where the observed peak concentrations were detected. By 1100 LT, some of the particles from this layer had mixed to the surface as the convective boundary layer grew to a height of 0.5 km AGL. There was also very little north-south variation in the

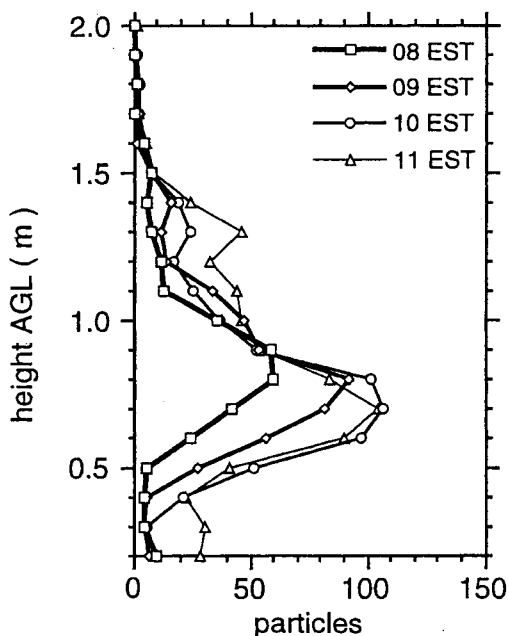


Figure 7. Simulated particle concentration profiles from by the RAMS/LPDM for a sampling volume around the G-1 flight paths, August 31, 1995.

particle concentration between 0800 and 1100 LT suggesting that mixing of pollutants from several source regions contributed to the layer over Connecticut and Massachusetts. The concentration profile over central Connecticut became more vertically uniform between 1100 and 1400 LT as turbulent diffusion continued to mix the particles within the convective boundary layer. Late in the afternoon, the particles released from New York during the morning entered the

sampling domain over Long Island Sound and southern Connecticut, so that the particle concentrations were no longer uniform in the north-south direction.

As shown in Figure 8a, most of the particles within the sampling domain at the time of the G-1 aircraft flights originated from New York and Philadelphia. However, the modeling system indicated that it would have been possible for emissions from the Lake Ontario region to be advected into the region. As a consequence of mixing from several sources, the particle profile in the morning does not have a unique "age," as would be expected from simple advection with no turbulent diffusion processes [Fast and Berkowitz, 1997], but is better characterized by a distribution of values as shown in Figure 8b. Most of the particles over Connecticut between 0800 and 1100 LT were released the previous day, with a relatively low percentage of the particles having a transport duration greater than 2 days.

The mechanism by which the layer was formed during the August 31 case is very similar to that postulated for ozone layers observed during the 1993 NARE field campaign [Fast and Berkowitz, 1996, 1997]. The role of boundary layer processes in defining the vertical distribution of pollutants was examined using a model formulation similar to that employed here. In the present NARSTO '95 simulations, the peak in the particle concentration profile (Figure 7) is associated with the development of well-mixed upwind urban boundary layers during the previous daytime periods in which the vertical potential temperature gradient becomes small and particles, as surrogates for an emission mix of  $\text{NO}_x$  and hydrocarbons, are transported upward as high as 2 km AGL. During the evening, particles located within the nocturnal residual layer between 0.5 and 1.5 km AGL over New York and Philadelphia are subsequently advected by higher wind speeds above the nocturnal boundary layer to Connecticut and Massachusetts by the next morning, August 31. The minimum in particle concentration near the surface is associated

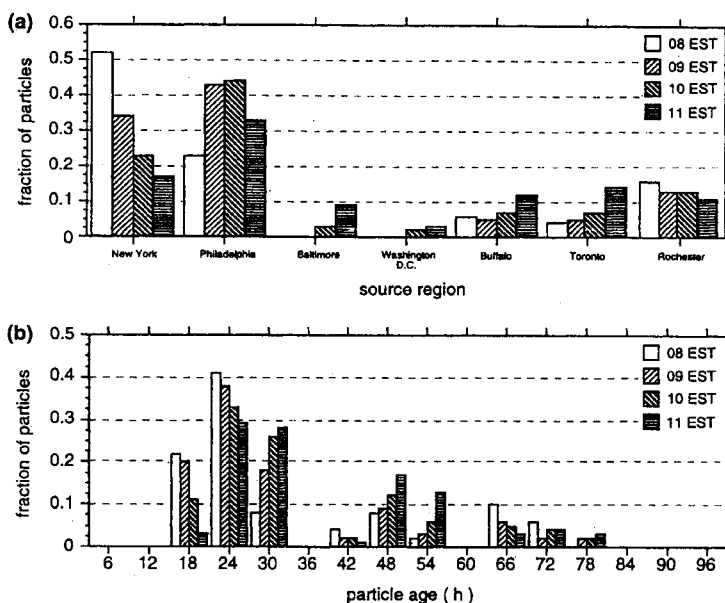


Figure 8. Simulated (a) source regions and (b) age of particles within the sampling volume along the G-1 flight segment between 0800 and 1100 LT, August 31, 1995.

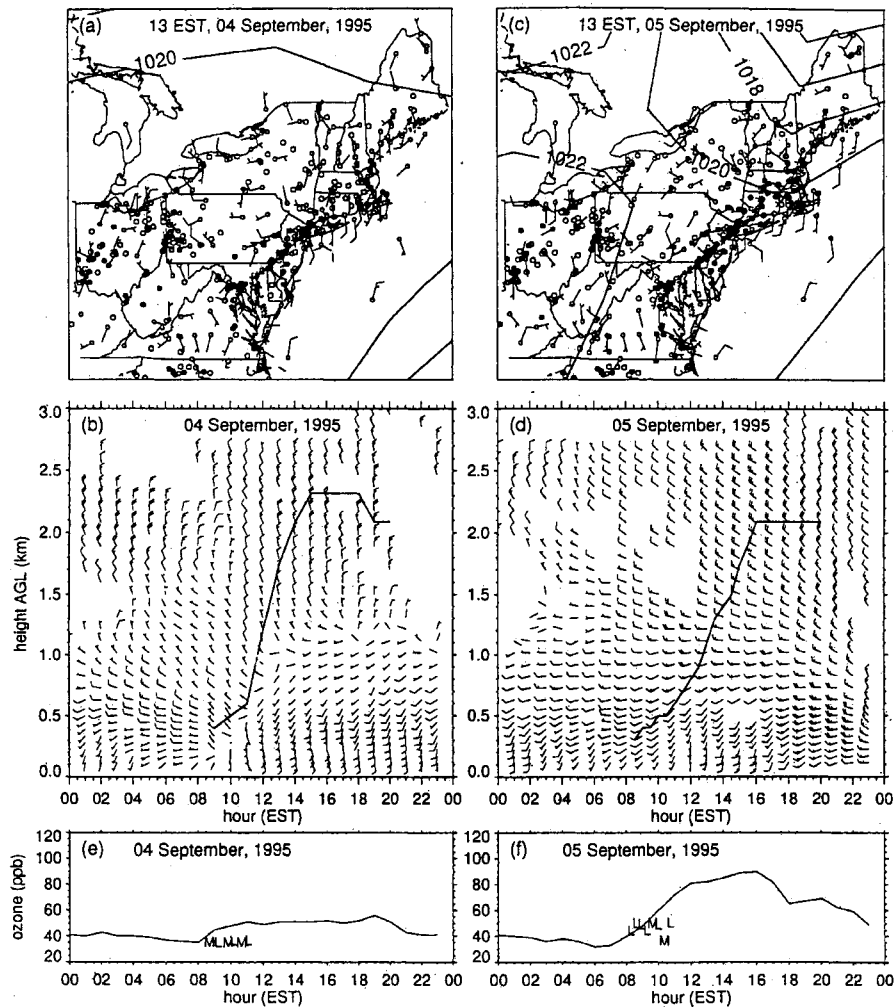


Figure 9. Same as Figure 2, but for September 4 and 5, 1995.

with the suppression of upwind vertical diffusion at night so that only particles (as surrogates for pollutants) within the nocturnal stable layer are transported. Additional details of this mechanism are given by *Fast and Berkowitz* [1996].

#### 4.2. Case 2: September 4-5

A persistent ridge over the eastern United States several days prior to September 5 resulted in light surface and upper air winds and mostly clear to partly cloudy skies. The near-surface winds at Millstone Point during the afternoon of September 4 were southerly and usually less than  $5 \text{ m s}^{-1}$  (Figure 9b). Also shown in Figure 9b is the simulated mixed layer height. The model predicted a deep convective boundary layer on September 4, with a mixed layer height of approximately 2.3 km AGL between 1500 and 1800 LT.

Light southwesterly winds were observed near the surface during the morning of September 5 (Figure 9d); however, as with the August 31 event, the near-surface winds grew in intensity with speeds as strong as  $15 \text{ m s}^{-1}$  at about 0.5 km AGL by 2000 LT. An upper level trough over Quebec produced somewhat stronger northwesterly flow aloft over

Connecticut during the afternoon of September 5. The mixed layer height was simulated to grow at a slower rate on September 5 reaching a maximum height that was 0.2 km lower than on September 4 (Figure 9b). As in the August 31 event, the growth of the convective boundary layer was slower and the maximum mixed layer heights were lower than the previous afternoon. The near-surface onshore flow on both days suggests that the boundary layer at Millstone Point was influenced by stable marine air. As in the August 31 event, the strong southwesterly winds during the afternoon of September 5 were due to the coupling of the large-scale pressure gradient (Figure 9c) and the onshore flow associated with a sea-breeze circulation.

The variation in the surface ozone mixing ratio observed at Worcester on September 4 (Figure 9e) was much less than those observed on September 5 (Figure 9f), analogous to the differences already noted between August 30 and 31. However, the synoptic patterns of September 4 and 5 (Figures 9a and 9c) are quite similar, in contrast to the differences observed for August 30 and 31. Aircraft sampling was carried out during the morning within a stratified atmosphere

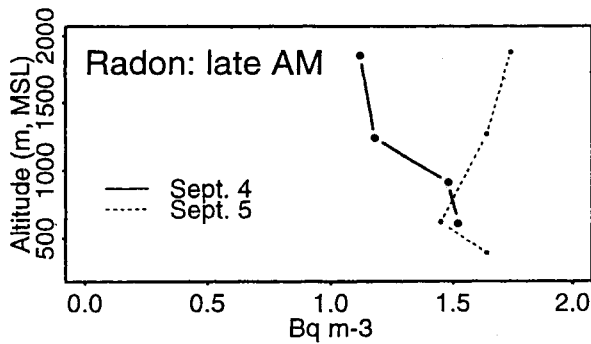


Figure 10. Radon profiles constructed from flight segments made after 0930 LT for September 4 and 5, 1995.

under conditions of light northerly upper level flow on September 4 and under northwesterly upper level flow on September 5.

A radon profile constructed from flight segments made after 0930 LT on the morning of September 4 shows values above 1 km to be less than  $1.5 \text{ Bq m}^{-3}$  (Figure 10). National Weather Service temperature profiles made the previous afternoon (1900 LT, September 3) suggest a mixed layer height over the region of  $\sim 1 \text{ km}$ , which would have limited the upward mixing of radon to this altitude. A similar radon profile constructed from flight segments made after 0930 LT on the morning of September 5 resulted in values that were greater than  $1.5 \text{ Bq m}^{-3}$  above 1.5 km, consistent with the  $\sim 1.5 \text{ km}$  mixing layer height of September 4. Assuming that the surface flux of radon was the same on September 4 and 5, a smaller concentration aloft would be expected with mixing

through a shallow layer on the preceding day relative to days preceded by a deeper mixed layer. Zaucker *et al.* [1996] postulated that variations in mixing layer height are the prime factor in determining radon concentrations in the free atmosphere. This hypothesis appears to be supported by the present data.

The atmosphere during the early morning hours of September 5 showed a vertical gradient in convective activity, as seen in the profile of the variance of the high-frequency potential temperature,  $\sigma^2_{\theta}$  (Figure 11; top left). However, unlike the August 31 profile, ozone mixing ratios greater than those observed at the surface extended to the highest flight segment at approximately 2000 m MSL. The moisture and  $\text{NO}_y$  levels decreased with altitude, while ozone mixing ratios were relatively uniform aloft ( $\sim 60 \text{ ppb}$ ) and 1.5 times greater than those observed during the lowest altitude segment ( $\sim 40 \text{ ppb}$ ).

The sustained synoptic scale subsidence, deeper layers of uniform ozone and CO levels, and a persistent ridge of high pressure over the region suggest that the profiles in Figure 11 are associated with an air mass that has undergone extensive photochemical aging compared to the layer detected on August 31.  $\text{NO}_y$  levels at  $\sim 400 \text{ m}$ , MSL (Figure 5b) were almost twice those measured on August 31 due primarily to a doubling of  $\text{NO}_x$  mixing ratios, while PAN (Figures 5b and Figure 12) and  $\text{HNO}_3$  had similar values. Nitric acid measurements taken concurrent with the PAN observations in the aged layer of September 5 were 60% greater than those measured in the relatively younger layer of August 31, consistent with  $\text{HNO}_3$  being considered an end product of many chemical reaction chains.

The NMHC sampling during the morning of September 5 consisted of canisters at only three altitudes, with two of them

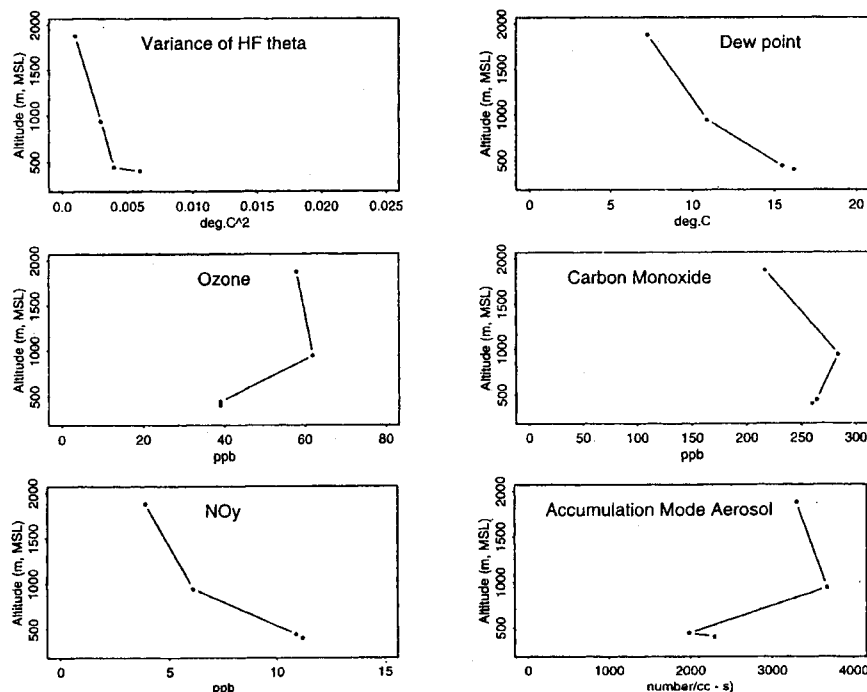
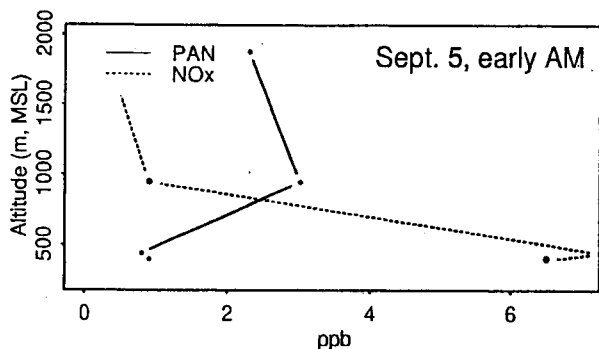


Figure 11. Profiles of mean values measured along the flight segments of September 5, 1995 (see Figure 3). Values are plotted for flight segments 8, 4, 6, and 2.



**Figure 12.** Vertical profile PAN and  $\text{NO}_x$  ( $=\text{NO} + \text{NO}_2$ ), September 5, segments 8, 4, 6, and 2 (see Tables 1 and 2).

relatively close to each other. Low-altitude mixing ratio of NMHCs on this date were similar to those noted for August 31, with ethane being dominant at the three altitudes, followed by propane. Isoprene dominated in propene-equivalent reactivity at the two lowest layers, with reactivities an order of magnitude greater than the second most reactive compound (ethene).

The profiles derived from the particle dispersion simulation for the morning hours of September 5 are shown in Figure 13. The origin of this layer was again related to the development of a well-mixed boundary layer during the daytime of the previous day in regions upwind of the sampling domain. Particles remaining within the residual layer were transported during the night over the nocturnal stable boundary layer. The modeling system produced peak concentrations between 0.5 and 0.7 km AGL, an elevation lower than the observed layer. In contrast to the event on August 31, a significant fraction of the particles were simulated to be in the sampling domain at altitudes greater than 1.5 km AGL. These model results were consistent with the aircraft measurements that also had relatively high concentrations and very little north-south variation at 2 km AGL between 0800 and 1100 LT. The simulated particle profile over central Connecticut became more uniform in the vertical between 1100 and 1400 LT as turbulent diffusion continued to mix the particles within the convective boundary layer. At 1100 LT, after aircraft sampling was terminated, a significant number of particles were simulated to enter the sampling domain over Long Island Sound and southern Connecticut, so that the particle concentrations were no longer uniform in the north-south direction.

Most of the simulated particles within the sampling domain at the time of the G-1 aircraft flights on September 5 originated from New York, Philadelphia, Baltimore, Washington D.C., Cleveland, and Pittsburgh (Figure 14a); however, a small fraction of the particles originated from other areas along the Great Lakes. A greater number of source regions contributed to the particles in the area on September 5 than on August 31. In contrast to August 31, when many particles had residence times of 30 hours or less, a wide distribution of ages was determined by the modeling system on September 5, with a large fraction of the particles taking 2 days of transport to reach Connecticut (Figure 14b). This is due to the synoptic conditions during the period in which persistent high pressure is situated over the northeastern United States with associated low wind speeds.

## 5. Summary and Conclusions

Meteorological observations from wind profilers throughout the northeast have been combined with surface and airborne chemical measurements to describe the synoptic and regional-scale circulations on 2 days during which surface ozone mixing ratios on the east coast of the United States exceeded 90 ppb. The RAMS and LPDM models were used in conjunction with these observations to describe the atmospheric features that affect pollutant transport and diffusion during the sampling period.

A total of six airborne missions were flown between August 30 and September 5, 1995, in which instrumentation onboard the G-1 measured chemical and meteorological quantities during a series of horizontal flight segments at various altitudes below 2 km over eastern Connecticut and central Massachusetts. Sampling alternated within and above the developing mixed layer. Surface ozone measurements at Worcester were greater than 90 ppb on 2 days, August 31 and September 5, during this period. Vertical profiles of ozone, CO, aerosol, and  $\text{NO}_x$  over Worcester indicated the presence of residual pollutant aloft. The ratio of benzene to toluene within one of these layers suggested that vehicle emissions made a substantial contribution to the hydrocarbon mix aloft. On August 31, early morning sampling showed isoprene to be present only at the lowest sampling flight segment (393 m MSL). Later in the morning, the propene-equivalent mixing ratio of isoprene was an order of magnitude greater than the second most reactive NMHC (propene) at or below 650 m MSL.  $\text{NO}_x$  was found to be highly variable in both the vertical and horizontal. A sharp gradient in  $\text{NO}_x$  was observed across the mixed layer on days with high surface ozone mixing ratios, with  $\text{NO}_x$  values aloft being  $\sim 0.1$  ppb, in contrast to surface values of  $\sim 5$  ppb.  $\text{NO}_x$  was also found to make a smaller contribution to the total  $\text{NO}_y$ , with increased

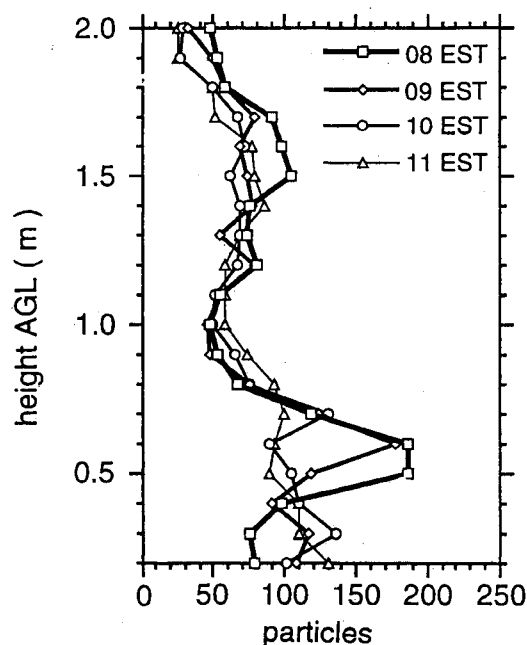


**Figure 13.** Simulated particle concentration profiles from by the RAMS/LPDM for a sampling volume around the G-1 flight paths, September 5, 1995.

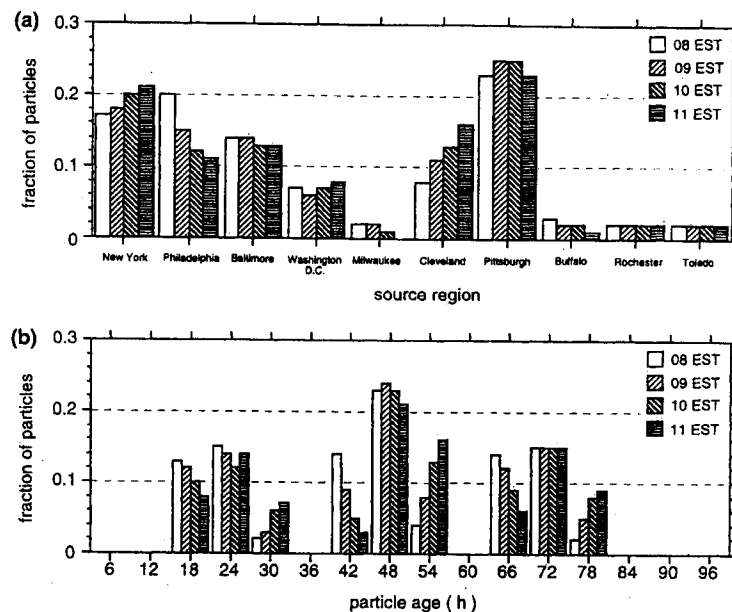


**Figure 14.** Simulated (a) source regions and (b) age of particles within the sampling volume along the G-1 flight segment between 0800 and 1100 LT, September 5, 1995.

altitude, although PAN contributed up to 50% of the total  $\text{NO}_x$  within the layers. It would therefore appear that PAN could provide a significant reservoir of additional  $\text{NO}_x$  and hence ozone, should these layers be mixed to the surface.

The high surface ozone mixing ratios observed on August 31 and September 5 differed from the days immediately preceding in two respects. First, no pollutant layers were detected above the growing convective boundary layer during the morning hours on the preceding days. Second, Worcester reported smaller values of ozone throughout the preceding days showed little diurnal variation. We attribute these differences to changes in the local circulation patterns that affected not only the chemical mix of air coming into the sampling domain, but also the mixed layer characteristics.

Southwesterly winds on the afternoon of August 31, the first of two high ozone occurrences, brought in a layer of photochemically aged pollutants from along the urban corridor southwest of the sampling domain. This layer appears to have formed from the diurnal sequence of boundary layer growth and mixing upwind of Connecticut. The peaks in distribution are associated with the development of deep, well-mixed boundary layers during the daytime in which the vertical potential temperature gradient becomes small and simulated particles (as surrogates for ozone and predecessor species) are transported upward as high as 2 km AGL. Results from the particle dispersion model suggest the layers of ozone, CO,  $\text{NO}_x$ , PAN, aerosols, and NMHC aloft were brought to the surface with the onset of convection. As a consequence of mixing from several sources, the profiles did not have a unique "age," but are better characterized by a distribution of values, with most of the particles over Connecticut released the previous day.

The September 5 case showed a relatively weak maximum above the top of the mixed layer in species associated with a more aged photochemical mix. In contrast to August 31, dur-

ing which most the transport duration of the particles was 30 hours or less, a wider distribution of ages was determined by the modeling system for the September 5 case study. We associate this feature with persistent high pressure that was situated over the northeastern United States, resulting in relatively low wind speeds in the study area. Most of the particles simulated to be within the sampling domain at the time of the G-1 aircraft flights on September 5 originated from New York, Philadelphia, Baltimore, Washington D.C., Cleveland, and Pittsburgh with a small fraction of the particles originating from other areas along the Great Lakes. The source region encompasses a much larger geographic domain for this case than was found for August 31.

A complete analysis of these measurements must await study with a comprehensive mesoscale/chemical model having a time and spatial resolution comparable to these observations. Such an analysis should explain the height variations noted in the component species of  $\text{NO}_x$  and quantitatively estimate the effect on surface ozone when PAN within photochemically aged layers is brought to the surface through convective mixing. Additional observations from rawinsondes, wind profilers, and surface air chemistry sites directly below the path of an aircraft measuring the compounds discussed in this paper during both the predawn and early morning hours would improve our understanding of how elevated layers of pollutants affect surface air chemistry.

Our initial analysis of the data describes the role of layering of ozone and ozone precursors located above the growing convective boundary layer on surface air chemistry. Such layers, created when pollutants are lofted into the upper part of the mixed layer through afternoon convective mixing in urban centers on previous days, are transported overnight into the Connecticut region. Elevated layers of ozone and ozone precursors that are entrained into the growing convective boundary layer may degrade surface air quality. These layers cannot be detected by standard surface air

quality monitoring stations; however, the aircraft observations suggest that they frequently form over the northeastern United States during the summer. This suggests that a significant portion of ozone at a particular location may be due to ozone and ozone precursors imported from distant sources.

**Acknowledgments.** The authors extend their thanks to pilots Bob Hannigan and Mike Warren for their invaluable input in the planning and safe execution of the flight plans for this study; to DOE's Research Aircraft Facility (Rich Barchet (manager) and Vic Morris); Yang Zhang (PNNL) for providing rate constants for use in the analysis of hydrocarbons; to the ground support crew of Malloy Air East of Suffolk County Airport / Gabreski Field; and to the NARSTO-Northeast Project Coordination Office for their assistance in providing the surface observations and profiler data used in this work. Funding for this work was provided by the U.S. Department of Energy's Atmospheric Chemistry Program. Pacific Northwest National Laboratory is operated for the U.S. Department of Energy by Battelle Memorial Institute under contract DE-AC06-76RLO 1830.

## References

- Berkowitz, C. M., and W. J. Shaw, Airborne measurements of boundary layer chemistry during the SOS: A case study, *J. Geophys. Res.*, **102**, 12,795-12,804, 1997.
- Berkowitz, C. M., K. M. Busness, E. G. Chapman, J. M. Thorp, and R. D. Saylor, Observations of depleted ozone within the boundary layer of the western North Atlantic, *J. Geophys. Res.*, **100**, 11,483-11,496, 1995.
- Carter, W. P. L., A detailed mechanism for the gas-phase atmospheric reactions of organic compounds, *Atmos. Environ., Part A*, **24**, 481-518, 1990.
- Carter, W. P. L., and R. Atkinson, An experimental study of incremental hydrocarbon reactivity, *Environ. Sci. Technol.*, **21**, 670-679, 1987.
- Carter, W. P. L. and R. Atkinson, Computer modeling study of incremental hydrocarbon reactivity, *Environ. Sci. Technol.*, **23**, 864-880, 1989.
- Chameides, W. L., et al., Ozone precursor relationships in the ambient atmosphere, *J. Geophys. Res.*, **97**, 6037-6055, 1992.
- Daum, P. H., L. I. Kleinman, L. Newman, W. T. Luke, J. Weinstein-Lloyd, C. M. Berkowitz, and K. M. Busness, Chemical and physical properties of plumes of anthropogenic pollutants transported over the North Atlantic during the North Atlantic Regional Experiment, *J. Geophys. Res.*, **101**, 29,029-29,042, 1996.
- Davidson, W. R., S. Nacson, D. A. Lane, and B. A. Thomson, Ambient air analysis of inorganic acids and elemental halogens by atmospheric pressure chemical ionization, paper presented at 73<sup>rd</sup> Annual Meeting, Air Pollut. Control Assoc., Montreal, Quebec, Canada, 1980.
- DeMore, W. B., S. P. Sander, D. M. Golden, R. F. Hampson, M. J. Kurylo, C. J. Howard, A. R. Ravishankara, C. E. Kolb, and M. J. Molina, Chemical kinetics and photochemical data for use in stratospheric modeling, *JPL Publi.* 94-26, 1994.
- Dickerson, R. R., and A. C. J. Delany, Modification of a commercial gas filter correlation CO detector for enhanced sensitivity, *J. Atmos. Oceanic Technol.*, **5**, 424-432, 1988.
- Doskey, P. V., The effect of treating air samples with magnesium perchlorate for water removal during analysis for nonmethane hydrocarbons, *J. High Resolut. Chromatogr.*, **14**, 724-728, 1991.
- Doskey, P. V., and J. S. Gaffney, Nonmethane hydrocarbons in the Arctic atmosphere at Barrow, *Alaska, Geophys. Res. Lett.*, **19**, 381-384, 1992.
- Fast, J. D., Mesoscale modeling in areas of highly complex terrain, *J. Appl. Meteorol.*, **34**, 2762-2782, 1995.
- Fast, J. D., and C. M. Berkowitz, A modeling study of boundary layer processes associated with ozone layers during the 1993 North Atlantic Regional Experiment, *J. Geophys. Res.*, **101**, 28,683-28,699, 1996.
- Fast, J. D., and C. M. Berkowitz, Evaluation of back trajectories associated with ozone transport during the 1993 North Atlantic Regional Experiment, *Atmos. Environ.*, **31**, 825-837, 1997.
- Fehsenfeld, F. C., M. Trainer, D. D. Parrish, A. Volz-Thomas, and S. Penkett, North Atlantic Regional Experiment 1993 summer intensive: Forward, *J. Geophys. Res.*, **101**, 28,869-28,875, 1996.
- Fukui, Y., and P. V. Doskey, An enclosure technique for measuring nonmethane organic compound emissions from grasslands, *J. Environ. Qual.*, **25**, 601-610, 1996.
- Hanna, S. R., G. E. Moore, and M. E. Fernau, Evaluation of photochemical grid models (UAM-IV, UAM-V, and the ROM/UAM-IV Couple) using data from the Lake Michigan Ozone Study (LMOS), *Atmos. Environ.*, **30**, 3265-3279, 1996.
- Holdren, M. W., and C. W. Spicer, Field compatible calibration procedure for peroxyacetyl nitrate, *Environ. Sci. Technol.*, **18**, 113-116, 1984.
- Kleinman, L. I., P. H. Daum, Y.-N. Lee, S. R. Springston, L. Newman, W. R. Leitch, C. M. Banic, G. A. Isaac, and J. I. MacPherson, Measurements of O<sub>3</sub> and related compounds over southern Nova Scotia, I, Vertical distribution, *J. Geophys. Res.*, **101**, 29,043-29,060, 1996.
- Korc, M., P. Roberts, and D. Blumenthal, NARSTO-Northeast data management, report prepared by Sonoma Technology, Inc. for the Electric Power Research Institute, Palo Alto, California, 1996.
- Lee, H. N., and R. J. Larsen, Vertical diffusion in the lower atmosphere using aircraft measurements of <sup>222</sup>Rn, *J. Appl. Meteorol.*, **36**, 1262-1270, 1997.
- Negro, V. C., N. Y. Chiu, R. J. Larsen, S. B. Wurms, and C. Breheny, Continue testing and evaluation of the Radgrabber, EML 1995 annual report, *USDOE Rep. EML-580*, U.S. Dep. of Energy, Washington, D.C., 1996. (Available from Nat. Tech. Inf. Serv., U.S. Dep. of Commer., Springfield, Virginia).
- Nunnenmacher, L. J., Calibration and detection techniques for trace nitrogen compounds in the atmosphere, Ph.D. dissertation, Univ. of Md., College Park, 1990.
- Pielke, R. A., et al., A comprehensive meteorological modeling system - RAMS, *Meteorol. Atmos. Phys.*, **49**, 69-91, 1992.
- Roberts, P. I., M. Korc, D. Blumenthal, and P. K. Mueller, Description of the NARSTO-northeast 1995 summer ozone study, NARSTO-Northeast Proj. Coord. Off., Electr. Power Res. Inst., Palo Alto, California, 1995.
- Rogaski, C. A., D. M. Golden, and L. R. Williams, Reactive uptake and hydration experiments on amorphous carbon treated with NO<sub>2</sub>, SO<sub>2</sub>, O<sub>3</sub>, HNO<sub>3</sub>, and H<sub>2</sub>SO<sub>4</sub>, *Geophys. Res. Lett.*, **24**, 381-384, 1997.
- Sistla, G., N. Zhou, W. Hao, J.-Y. Ku, S. T. Rao, R. Bornstein, F. Freedman, and P. Thunis, Effects of uncertainties in meteorological inputs on urban airshed model predictions and ozone control strategies, *Atmos. Environ.*, **30**, 2011-2025, 1996.
- Spicer, C. W., W. J. Shaw, K. M. Busness, E. G. Chapman, and D. V. Kenny, A laboratory in the sky: New frontiers in measurements aloft, *Environ. Sci. Technol.*, **28**, 412A-420A, 1994a.
- Spicer, C. W., D. V. Kenny, G. F. Ward, I. H. Billick, and N. P. Leslie, Evaluation of NO<sub>x</sub> measurement methods for indoor air quality applications, *J. Air Waste Manage. Assoc.*, **44**, 163-168, 1994b.
- Zaucker, F., P. H. Daum, U. Wetterauer, C. M. Berkowitz, B. Kromer, and W. Broecker, Atmospheric <sup>222</sup>Rn measurements during the 1993 NARE intensive, *J. Geophys. Res.*, **101**, 29,149-29,164, 1996.

C. M. Berkowitz, J. D. Fast, and J. M. Hubbe, Pacific Northwest National Laboratory, Richland, WA 99352 (e-mail: cm\_berkowitz@pnl.gov; jd\_fast@pnl.gov; jm\_hubbe@pnl.gov)

P. V. Doskey, Argonne National Laboratory, Argonne, IL 60439 (e-mail: pvdoskey@anl.gov)

R. J. Larsen, Environmental Measurements Laboratory, New York, NY 10014 (e-mail: larsenr@eml.doe.gov)

R. Plastringer and C. W. Spicer, Battelle Memorial Institute, Columbus, OH 43201 (e-mail: plastringer@battelle.org; spicerc@battelle.org)

S. R. Springston, Brookhaven National Laboratory, Upton, NY 11973 (e-mail: srspringston@bnl.gov)

(Received September 18, 1997; revised December 18, 1997; accepted December 23, 1997.)